Global soil moisture retrieval from a synthetic L-band brightness temperature data set

Thierry Pellarin, Jean-Pierre Wigneron, Jean-Christophe Calvet, Philippe Waldteufel

Global soil moisture retrieval from a synthetic L-band brightness temperature data set

Thierry Pellarin,[1] Jean-Pierre Wigneron,[2] Jean-Christophe Calvet,[1] and Philippe Waldteufel[3]

Received 6 November 2002; revised 22 January 2003; accepted 10 March 2003; published 25 June 2003.

[1] A technique to retrieve surface soil moisture was assessed at the global scale using a synthetic data set of L-band (1.4 GHz) brightness temperatures T_B for 2 years, 1987 and 1988. The global T_B database consists of half-degree continental pixels and accounts for within-pixel heterogeneity, on the basis of 1 km resolution land cover maps. The retrievals were performed using a three-parameter inversion method applied to the L-band Microwave Emission of Biosphere model (L-MEB). Three land surface variables were retrieved simultaneously from the multiangular and dual-polarization T_B data: surface soil moisture *wg*, vegetation optical depth τ, and surface temperature T_S. The retrievals were obtained in two T_S configurations: T_S was either unknown or known with an uncertainty of 2 K. Applying these two assumptions, global maps of the estimated accuracy of the *wg* retrievals were produced, and the capability of the T_B to monitor *wg* was evaluated. A sensitivity study was carried out in order to analyze the effect of the main parameters that may affect the retrieval accuracy: the fraction cover of open water and forests, frozen soil conditions, and the radiometric noise on T_B. These results contribute to the better definition of the potential of the observations from future spaceborne missions such as the Soil Moisture and Ocean Salinity (SMOS) project. *INDEX TERMS:* 1640 Global Change: Remote sensing; 1866 Hydrology: Soil moisture; 3360 Meteorology and Atmospheric Dynamics: Remote sensing; *KEYWORDS:* L-band radiometry, soil moisture, inversion, modelling, global scale

Citation: Pellarin, T., J.-P. Wigneron, J.-C. Calvet, and P. Waldteufel, Global soil moisture retrieval from a synthetic L-band brightness temperature data set, *J. Geophys. Res.*, *108*(D12), 4364, doi:10.1029/2002JD003086, 2003.

1. Introduction

[2] In order to achieve a suitable spatial resolution at L-band, the possibility of using an antenna synthesis method was proposed. Such a concept relying on a deployable structure has led to the Soil Moisture and Ocean Salinity (SMOS) mission, which was the second Earth Explorer Opportunity Mission selected by the European Space Agency (ESA) in 1999. The SMOS mission [*Kerr et al.*, 2001] is scheduled for launch in 2006. The main objective of this mission is to deliver key state variables of land surfaces (soil moisture fields), and of ocean surfaces (sea surface salinity fields) with a ground resolution better than 50 km. The sensor consists of an interferometric radiometer that will provide dual-polarized, multiangular observations, with a high sampling time (3 days or better) and a global coverage.

[3] The root-zone soil moisture is a key variable of the water and energy exchanges at the land-surface/atmosphere interface, because it is a slowly varying quantity conditioning plant transpiration and bare soil evaporation [*Noilhan and Calvet*, 1995; *Wood et al.*, 1995]. Estimating this variable at the global scale has potential applications in hydrology and meteorology [*Fennessy and Shukla*, 1999; *Dirmeyer*, 2000; *Leese et al.*, 2001]. Several studies showed that time series of surface soil moisture (*wg*) can be used to retrieve the root-zone soil moisture by using an assimilation algorithm [*Entekhabi et al.*, 1994; *Calvet and Noilhan*, 2000; *Wigneron et al.*, 2002a]. A number of airborne and ground-based experiments have shown that L-band passive microwave remotely sensed brightness temperatures (T_B) have great potential for providing estimates of *wg*. Therefore the assimilation of T_B or of T_B-derived *wg* may permit to monitor the root-zone soil moisture. The objective of the assimilation is to retrieve variables which are not directly observed by remote sensing, but which can be simulated by using a process model (e.g., an atmospheric model or a soil-vegetation-atmosphere transfer–SVAT-model). For example, the root-zone soil moisture cannot be directly observed by a remote sensing system, but it is physically related to *wg*, which has a direct effect on the L-band emission of the soil. The estimation of the root-zone soil moisture using L-band radiometry requires the use of a SVAT model, simulating the time variations of *wg*, coupled with a radiative transfer model (RTM) simulating the T_B [*Calvet and Noilhan*, 2000]. In this study, the SVAT model was used to build the synthetic data set, and was not involved

[1]Centre National de Recherches Météorologiques–Groupe d'Etude de l'Atmosphère Météorologique, Météo-France, Toulouse, France.
[2]Unité de Bioclimatologie, Institut National de la Recherche Agronomique, Villenave d'Ornon, France.
[3]Service d'Aéronomie, Institut Pierre Simon Laplace, Verrières le Buisson, France.

0148-0227/03/2002JD003086

in the retrieval exercise. The assimilation of remote sensing data to analyze surface fields like the root-zone soil moisture is currently not operational. There is a debate about which technique should be used to analyze surface variables: assimilate remote sensing products (obtained by inverting a RTM) or assimilate radiances by coupling the SVAT model with a RTM. Assimilation is beyond the scope of this study, which concerns RTM inversion only.

[4] On the basis of both large-scale airborne experiments over agricultural sites and ground-based experiments over crop fields, the potential of L-band radiometry to retrieve the surface soil moisture has been evaluated and retrieval algorithms have been proposed [*Wang et al.*, 1990; *Schmugge and Jackson*, 1994; *Jackson et al.*, 1995, 1999; *Van de Griend and Owe*, 1994; *Wigneron et al.*, 1995, 2000; *Njoku and Li*, 1999; *Owe et al.*, 2001]. However, as extensive L-band observations from spaceborne systems are not currently available, these various soil moisture retrieval approaches could not be assessed at the global scale.

[5] In the present study we used a global data set of synthetic T_B, at L-band, computed for a two-year period, 1987 and 1988 (T. Pellarin et al., Two-year global simulation of L-band brightness temperatures over land, submitted to *IEEE Transactions on Geoscience and Remote Sensing*, 2003) (hereinafter referred to as Pellarin et al., submitted manuscript, 2003). This period presents a significant climatic variability: contrasting El-Niño and La-Niña climatic conditions prevailed in 1987 and 1988, respectively. The simple L-band Microwave Emission of Biosphere model (L-MEB; Pellarin et al. (submitted manuscript, 2003)) was used to produce the multitemporal, half-degree T_B maps at several incidence angles and for horizontal and vertical polarizations (H and V, respectively). Synthetic or semi-synthetic (based on a combination of measured and simulated data) data sets are routinely used in defining new space missions at the European Space Agency (ESA). Such data sets have proved to be very useful for the design of the instrument and for the definition of the orbit and ground segment (system preprocessing, calibration procedures, atmospheric corrections, retrieval concepts, etc.) of the spatial mission. This kind of approach is all more justified in the case of SMOS by the lack of alternative L-band spaceborne measurements corresponding to real-world data. Furthermore, the methods used in this study (direct modeling and inversion process) were developed and validated from ground- and airborne-based measurements. They should be valid to analyze spaceborne measurements in the case of SMOS as: (1) Atmospheric effects are very low. Both downward and upward atmospheric brightness temperatures are in the range of 1 to 3 K at nadir (i.e., about 1% of the total T_B), depending mainly on air temperature and atmospheric pressure. Clouds have virtually no effect on the atmosphere absorption at L-band. (2) Measurements are not sensitive to illumination conditions. (3) The global emission of heterogeneous scenes can be easily computed as the sum of contributions of all surface types, weighted by the fraction of surface cover. (4) Complex effects in relation with geometry (vegetation structure, surface roughness, . . .) have much less impact at large spatial scale as there is some kind of compensation due to the mixing of a variety of contributions to the emitted signal as found in the analysis of active spaceborne microwave measurements [*Cognard et al.*, 1995].

[6] The synthetic global T_B data set obtained by Pellarin et al. (submitted manuscript, 2003) was a useful reference to develop and validate methods to retrieve soil moisture. On the basis of these T_B data, the retrieval of *wg* using simple statistical regression algorithms [*Pellarin et al.*, 2003] was investigated. In the most promising of these approaches, referred to as the Local Regression Model (LRM), independent regression models were calibrated over each pixel. Satisfactory results were obtained and the accuracy of the LRM soil moisture retrieval was better than 0.04 $m^3\ m^{-3}$ over about 90% of the continental area (note that the 0.04 $m^3\ m^{-3}$ threshold was considered as the required accuracy of *wg* retrievals [*Kerr et al.*, 2001]).

[7] This paper describes the results obtained using a different retrieval method, forward model inversion, which was evaluated using the same synthetic L-band global data set. This method was derived from the inversion algorithm proposed by *Wigneron et al.* [2000]. The retrievals were obtained by the inversion of L-MEB, and two inversion configurations were tested, assuming that surface temperature was either unknown or known with an uncertainty of 2 K. Global maps of the estimated accuracy of the soil moisture retrievals were produced and the capability of L-band T_B observations to monitor *wg* could be evaluated in the two situations. A sensitivity study was carried out to analyze the effect of the main parameters that may affect the retrieval accuracy: the fraction cover of open water and forests, soil freezing, and the radiometric noise on T_B.

2. Material and Methods

[8] This study is based on a global data set including synthetic L-band brightness temperatures and the associated land surface characteristics during a two-year period from 1 January 1987 to 31 December 1988. A detailed description of the data set and of the modeling approaches used to carry out the simulations is given by Pellarin et al. (submitted manuscript, 2003). In this section, the main features of the data set and of the L-MEB model are summarized and the model inversion method is presented.

2.1. Synthetic Data Set

[9] The simulations were performed using a two-step process:

[10] 1. A land surface scheme, the Interactions between the Soil, the Biosphere and the Atmosphere (ISBA) model [*Noilhan and Planton*, 1989], was used at the global scale to simulate the time variations of the surface state characteristics (i.e., the soil temperature and moisture content at the surface and at depth, the snow cover characteristics) required by the L-band emission model. The simulations used two-year atmospheric forcing data derived from the International Satellite Land Surface Climatology Project Initiative I (ISLSCP I) data [*Meeson et al.*, 1995] and a detailed global surface database, ECOCLIMAP [*Masson et al.*, 2003], containing a global land cover map at a spatial resolution of 1 km.

[11] 2. The L-MEB model was used to produce multitemporal T_B maps from the ISBA outputs as well as from information derived from the ECOCLIMAP thematic maps and the atmospheric forcing database. The brightness temperatures were computed for five different incidence angles (0, 20, 30, 40 and 50°) and two polarizations (H and V).

Table 1. Main Input Variables of the L-Band Microwave Emission of Biosphere (L-MEB) Model[a]

Symbol	Definition	Unit
	Variables	
T_{AIR}	Air temperature (2m)	K
T_S	Skin surface temperature	K
T_2	Soil temperature	K
wg	Surface soil moisture	$m^3\ m^{-3}$
wg_I	Surface frozen soil moisture	$m^3\ m^{-3}$
w_R	Rain intercepted by the canopy	$kg\ m^{-2}$
h_{SNOW}	Snow depth	M
ρ_{SNOW}	Snow density	$kg\ m^{-3}$
T_{SNOW}	Snow temperature	K
$w_{SNOWliq}$	Liquid water content of the snow mantel	$kg\ m^{-2}$
Vwc	Vegetation water content	$kg\ m^{-2}$
	Vegetation and Soil Parameters	
ω	Vegetation L-band single scattering albedo	–
b	Ratio τ/Vwc	$m^2\ kg^{-1}$
Clay, *Sand*	Soil texture	%
ρ_d	Dry bulk soil density	$g\ cm^{-3}$
h_{SOIL}, Q_{SOIL}, N_{SOIL}	Soil effective roughness parameters	–

[a]The surface soil moisture (wg), the L-band vegetation optical thickness (τ), and, possibly, the surface temperature (T_S) are the variables to be retrieved.

[12] 3. ECOCLIMAP is a new global data set at a 1 km resolution intended to be used to initialize the SVAT schemes in meteorological and climate models, at all horizontal scales. The database supports the 'tile' approach, which is used by an increasing number of SVAT models. In ECOCLIMAP, 215 ecosystems were derived from the combination of existing land-cover and climate maps with satellite data. Monthly estimates of the surface parameters used in SVAT models, such as leaf area index (*LAI*), vegetation fraction, roughness length, minimal stomatal resistance, albedo and emissivity are provided by ECOCLIMAP, based on look-up tables. The high resolution of ECOCLIMAP (1 km) is useful for studies at much larger scales, because it provides the sub-grid information: different surface parameters can be assigned to, for example, the bare soil, low vegetation and woody vegetation fractions of the grid mesh, allowing the computation of several energy budgets for the same grid mesh.

[13] The synthetic L-band T_B were simulated at a half-degree resolution and at this rather coarse spatial resolution, few homogeneous pixels can be found. Therefore the sub-pixel heterogeneity was accounted for by using a "multi-patch" version of ISBA. This version was able to simulate distinct water and energy budgets in the same pixel for the three main surface types that were considered (namely bare soil, woody vegetation and herbaceous vegetation). ISBA was run at a spatial resolution of half a degree (about $50 \times 50\ km^2$) and produced daily 0600 and 1800 local standard time (LST) maps of the variables (wg and temperature, and snow characteristics) required for running the L-MEB model. A number of variables produced by ISBA or derived from the ISLSCP I and ECOCLIMAP data sets were stored daily for the two considered local times. These variables are listed in Table 1. For a given pixel, distinct simulations of the same variable were performed by ISBA, for each tile of the pixel.

[14] The spatial distribution of the four different land covers is given in Figure 1. Most pixels are heterogeneous since only 10% of them consist of a single cover type (mainly bare soil in Sahara). In ECOCLIMAP, the total forest area represents 29.2% of the continental surface (9.6, 5.2 and 14.4% of tropical, broadleaf and coniferous forests, respectively). Herbaceous vegetation represents 47.3% of the continental surface (12.9 and 34.4% of crops and grasslands, respectively). The bare soil surface type covers 23.5% of the continental areas. For more than 33% of the pixels, the surface fraction of open water exceeds 1%.

2.2. The L-MEB Model

[15] The L-MEB model is the result of an extensive review of the current knowledge of the microwave emission

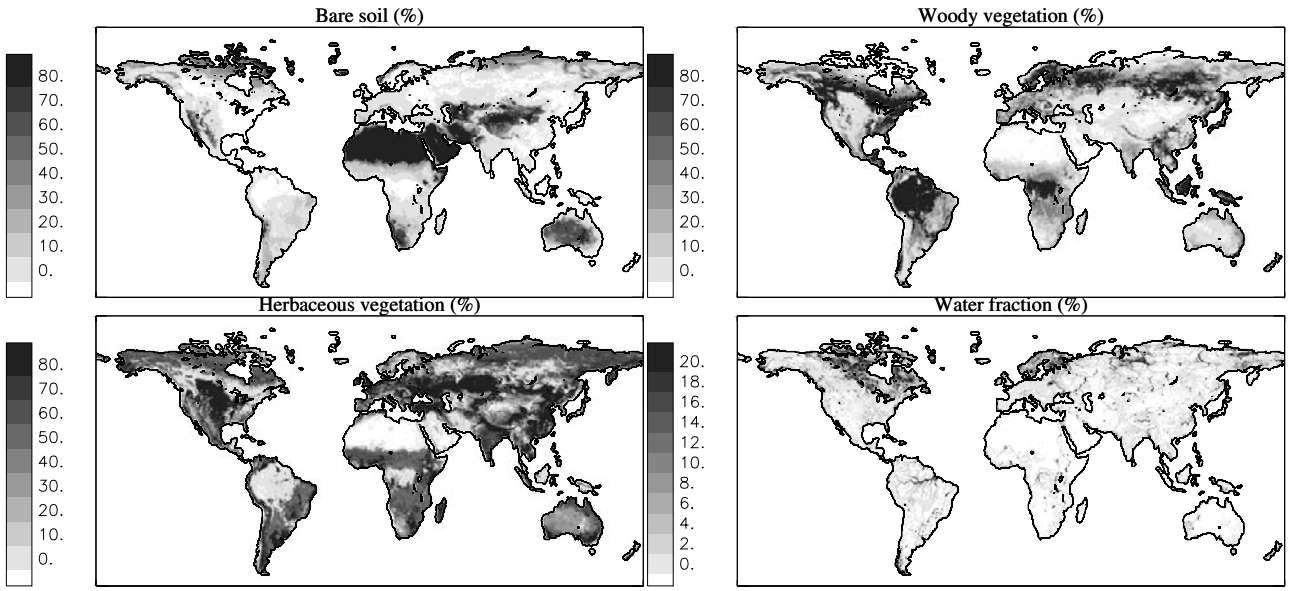

Figure 1. Global half-degree maps obtained from the ECOCLIMAP data set: fractional cover of bare soil, woody vegetation, herbaceous vegetation and free water surfaces.

of various land surface types (herbaceous and woody vegetation, frozen and unfrozen bare soil, snow, etc.) at L-band. The main components of L-MEB are (1) the vegetation module using the τ-ω approach [see, e.g., *Wigneron et al.*, 1995], (2) a snow emission model developed by *Pulliainen et al.* [1993] and *Pulliainen and Hallikainen* [2001], and (3) a simple parameterisation of the atmospheric effects (Pellarin et al., submitted manuscript, 2003). The main variables needed to simulate T_B are the *wg* and temperature, the vegetation water content, the soil roughness parameters, the soil type, and the snow mantel characteristics (depth, density, grain size, liquid water content). The air temperature and the surface elevation are also needed to simulate the atmospheric effects. The simulation process accounted for sub-pixel heterogeneity. Four main surface types, and the associated values of their cover fraction within each pixel, were considered: bare soil, herbaceous vegetation (grassland or crops), forests (coniferous, broadleaf or tropical forests), open water surfaces (lakes, river, . . .). For all of these cover types, the possible presence of snow was considered. It was assumed that snow covered bare soil and herbaceous vegetation surfaces. For forests, the snow layer was assumed to lie below the forest canopy. Situations of partially and/or totally frozen soil were accounted for by using different values of the soil dielectric permittivity. Also, open water surfaces could be frozen (in this case the dielectric permittivity of ice was used). The brightness temperature of the mixed pixel including all (or some of) the four surface types was written as:

$$T_{B(p,\theta)} = f_B \cdot T_{B_{(p,\theta)-B}} + f_F \cdot T_{B(p,\theta)-F} + f_H \cdot T_{B(p,\theta)-H} + f_W \cdot T_{B(p,\theta)-W} \quad (1)$$

where f_X is the cover fraction of the different surface types (X = B, F, H, W for bare soil, forests, herbaceous vegetation-covered surfaces, open water surfaces respectively), and $T_{B(p,\theta)-X}$ is the p-polarized brightness temperature at an incidence angle θ. The modeling of $T_{B(p,\theta)-X}$ also included the down-welling sky and cosmic radiation reflected by the surface.

[16] For both herbaceous and woody vegetation tiles, only the majority land cover was used (i.e., mixed grassland and crop landscapes or coniferous and broadleaf forests were not considered). For all the vegetation types, L-MEB rests on the vegetation single scattering albedo ω representing the scattering within the canopy layer and on the vegetation optical depth τ, which parameterizes the attenuation effects. The vegetation optical depth τ can be estimated using the so-called *b* parameter [*Jackson and Schmugge*, 1991]:

$$\tau = b\, VW_C \quad (2)$$

where VW_C (kg.m^{-2}) is the aboveground vegetation water content.

[17] A value of *b* of 0.12 ± 0.03 was reported as representative of most agricultural crops at 1.4 GHz [*Jackson and Schmugge*, 1991]. In the present study, for non-forested canopies, VW_C was related to *LAI* as $VW_C = 0.5\ LAI$. It follows that the optical depth of the low-vegetation canopies varied with time, like the monthly estimates of *LAI* derived from the ECOCLIMAP database. On the contrary, over forests, the value of τ was assumed to be constant and was related to the branch water content [*Ferrazzoli et al.*, 2002]. The vegetation parameters of the vegetation types are given in Table 2. In the case of forests, the highest optical depth ($\tau = 2$) was prescribed for tropical forests. The value of ω depends on the vegetation structure, which is mainly a function of the canopy type and phenology. To simulate T_B, significant simplifications were made, and ω was considered to be constant, with an average value of 0.05 and 0.15 for low-vegetation canopies and forests, respectively. However, the actual range of variations of ω is probably about 0–0.1 for low-vegetation covers and about 0.05–0.15 for forests. As, to date, it is impossible to build accurate global maps of ω, it was assumed that no a priori information was available about ω in the retrieval process and this parameter was set to a constant value of 0.05 (section 2.4).

Table 2. Value of the L-MEB Vegetation Parameters at the Global Scale[a]

Surface Type	Single-Scattering Albedo ω	*b* Parameter	Vegetation Water Content *Vwc*, kg m^{-2}
Grasslands	0.05	0.20	0.5 *LAI*
Crops	0.05	0.15	0.5 *LAI*
Rain forests	0.15	0.33	6 (branches)
Deciduous forests	0.15	0.33	4 (branches)
Coniferous forests	0.15	0.33	3 (branches)

[a]With leaf area index (*LAI*) values in units of m^2 m^{-2}.

[18] The effect of surface roughness on the soil emission was accounted for by using a simple formulation, which was found to be adequate for most applications. In this semi-empirical equation, the polarized soil reflectivity $\Gamma_S(\theta, p)$ is computed as a function of three empirical soil roughness parameters (h_{SOIL}, Q_{SOIL} and N_{SOIL}) [*Wang and Choudhury*, 1981]:

$$\Gamma_s(\theta,p) = [(1-Q_{SOIL})\Gamma_s^*(\theta,p) + Q_{SOIL}\Gamma_s^*(\theta,q)] \cdot \exp\left(-h_{SOIL}\cos(\theta)^{N_{SOIL}}\right) \quad (3)$$

where p and q stand for the polarization (V or H), and $\Gamma_S^*(\theta, p)$ is the polarized specular reflectivity which can be computed from the soil dielectric permittivity ε_S and the incidence angle θ, by using the Fresnel equations. A detailed analysis of the soil roughness effects performed by *Wigneron et al.* [2001] showed that both Q_{SOIL} and N_{SOIL} could be set equal to zero at L-band and that the L-band surface microwave emissivity can be written as:

$$e_p = 1 - \Gamma_s(\theta,p) = 1 - [\Gamma_s^*(\theta,p)\exp(-h_{SOIL})] \quad (4)$$

[19] In most soil moisture retrieval studies based on L-band airborne or ground-based experiments, roughness conditions were generally found to be rather smooth over agricultural or natural areas. In this study, for the sake of simplicity, the parameter h_{SOIL} was set constant and equal to 0.3, which is a value representative of rather smooth soil roughness conditions. The effects of topography were not considered in this study. It is expected that these effects are generally rather low except in mountainous regions where the capabilities of monitoring soil moisture are generally limited by dense forest covers.

[20] The validation of the main components of L-MEB was described in several papers. Many studies addressed the L-band emission of herbaceous canopies [*Mo et al.*, 1982; *Brunfeldt and Ulaby*, 1984; *Brunfeldt and Ulaby*, 1986; *Pampaloni and Paloscia*, 1986; *Van de Griend and Owe*, 1993; *Wigneron et al.*, 1995]. The validation of the simulation of forest and snow emission was described by *Ferrazzoli et al.* [2002], *Pulliainen et al.* [1999], and *Pulliainen and Hallikainen* [2001], respectively.

2.3. Model Inversion

[21] The three-parameter retrieval method used in this study consisted in retrieving three land surface variables simultaneously from the multiangular and dual-polarization T_B data: the surface soil moisture, the vegetation optical depth, and the surface temperature (wg*, τ*, and T_S^*, respectively, where * denotes retrieved values). The inversion process was based on a standard minimization routine computing the retrieved variables and the associated standard errors [*Wigneron et al.*, 2000]:

[22] 1. For each continental pixel, and each observation date (each day at 0600 and 1800 LST), a vector T_B^{ref}, representing the reference land surface emission for five incidence angles and two polarizations was extracted from the T_B data set.

[23] 2. A Gaussian noise with standard deviation σ_{TB} was added to T_B^{ref} in order to simulate an observed vector T_B^0, accounting for the uncertainties associated with the spaceborne measurements, in terms of radiometric sensitivity. Three levels of σ_{TB} were considered in this study: 1, 2 and 3 K. The 1 K noise level is consistent with the radiometric performance expected for SMOS and was considered as the reference value of the radiometric noise in this study. However, the effect of larger noise levels (2 and 3 K levels) was evaluated. In addition to the radiometric noise, a noise representative of the imperfect correction of the Faraday rotation was accounted for and was added to the synthetic T_B. Faraday rotation tends to depolarize the signal. In this study, this noise was lower than 0.5 K with a probability of 98% [*Pellarin et al.*, 2003].

[24] 3. The retrievals of wg, τ and T_S were obtained by minimizing a cost function (C_F). The minimization routine was a generalized least squares iterative algorithm [*Marquardt*, 1963] modified (P. Waldteufel and G. Caudal, unpublished manuscript, 2001) to account for a priori information available on model-input parameters: for example, first guess of wg, τ and T_S (wg^{ini}, τ^{ini} and T_S^{ini}), and the associated standard deviations σ_{wg}, σ_τ and σ_{Ts}. The routine produced both the retrieved surface parameters (wg, τ and T_S) and the theoretical estimates of the standard deviations associated with these retrievals, assuming that T_B^0 and the model-input parameters were affected by a Gaussian random error.

[25] The cost function (C_F) was the sum of the weighed squared differences between retrieved and observed values and reference and simulated T_B:

$$C_F = \frac{\sum\left[T_{Bp}(\theta_i) - T^o_{Bp}(\theta_i)\right]^2}{\sigma^2_{TB}} + \frac{(wg^* - wg^{ini})^2}{\sigma^2_{wg}} + \frac{(\tau^* - \tau^{ini})^2}{\sigma^2_\tau} + \frac{(T_S^* - Ts^{ini})^2}{\sigma^2_{Ts}} \quad (5)$$

where Σ denotes the sum over the five incidence angles and both polarizations.

Table 3. Selected Initial Values and Standard Deviations of the Three Parameters of the Inversion: Surface Soil Moisture, L-Band Optical Thickness of the Vegetation, and Surface Temperature[a]

	wg^{ini}, m^3 m^{-3}	σ_{wg}, m^3 m^{-3}	τ^{ini}	σ_τ	T_S^{ini}, K	σ_{Ts}, K
IP1	0.15	0.1	0.5	0.4	280	15
IP2	0.15	0.1	0.5	0.4	Ts ± 2	2

[a]The *ini* superscript denotes initial values; σ, standard deviations; wg, surface soil moisture; τ, L-band optical thickness; and T_S, surface temperature.

2.4. Two Inversion Approaches

[26] Two different retrieval approaches were tested. The first inversion process (referred to as IP1) was performed assuming that limited or no a priori information was available on the three parameters (wg, τ and T_S). In the second inversion process (referred to as IP2), T_S was assumed to be known with an uncertainty of 2 K.

[27] In the case of IP1, the values of wg^{ini}, τ^{ini}, T_S^{ini}, σ_{wg}, σ_τ, and σ_{Ts} were derived from the annual means and the associated standard deviations computed from the global data set. The obtained values are given in Table 3. The values of σ_{wg}, σ_τ, and σ_{Ts} are rather large, so that the retrieved values were almost independent from the initial values (wg^{ini}, τ^{ini} and T_S^{ini}).

[28] In IP2, the value of T_S^{ini} was taken as $T_S^{ref} + dT$, where dT is a term representing a Gaussian noise of 2 K, and σ_{TS} = 2 K (Table 3). The reason for using this configuration is that estimates of T_S may be obtained from thermal infrared remote sensing and/or global weather forecast analyses.

[29] In order to assess the performance of IP1 and IP2 in uncontrolled conditions, it was assumed that little a priori information on the pixel land cover was available. A number of assumptions were made:

[30] 1. In the forward model used in the inversion it was assumed that the land cover consisted of grassland. In particular the value of ω was set to 0.05 (Table 2). Since the optical depth was included in the inversion process the chosen value of b had no effect on the retrieval.

[31] 2. As discussed above, both N_{SOIL} and Q_{SOIL} were set equal to zero and the value of h_{SOIL} was set to a constant value of 0.3. This simplification may affects the representativeness of the retrieval process because in the real world, the roughness parameters may change from one pixel to another. However, preliminary tests have shown that the uncertainty affecting the roughness have little effect on the retrieved value of wg. On the other hand the retrieved values of τ may be perturbed by this effect.

[32] 3. The fractional cover of snow, open water and frozen soil was set to a nil value.

[33] 4. Soil texture was assumed to be equal to the mean global clay and sand fractions derived from ECOCLIMAP, 20.4 and 48.3%, respectively.

[34] 5. A nil vertical temperature gradient was assumed ($T_S = T_2$ in Table 1).

[35] Daily retrievals were obtained for 1988 (similar results were obtained for 1987 and are not presented here). The retrievals were carried out only at 0600 LST, which is

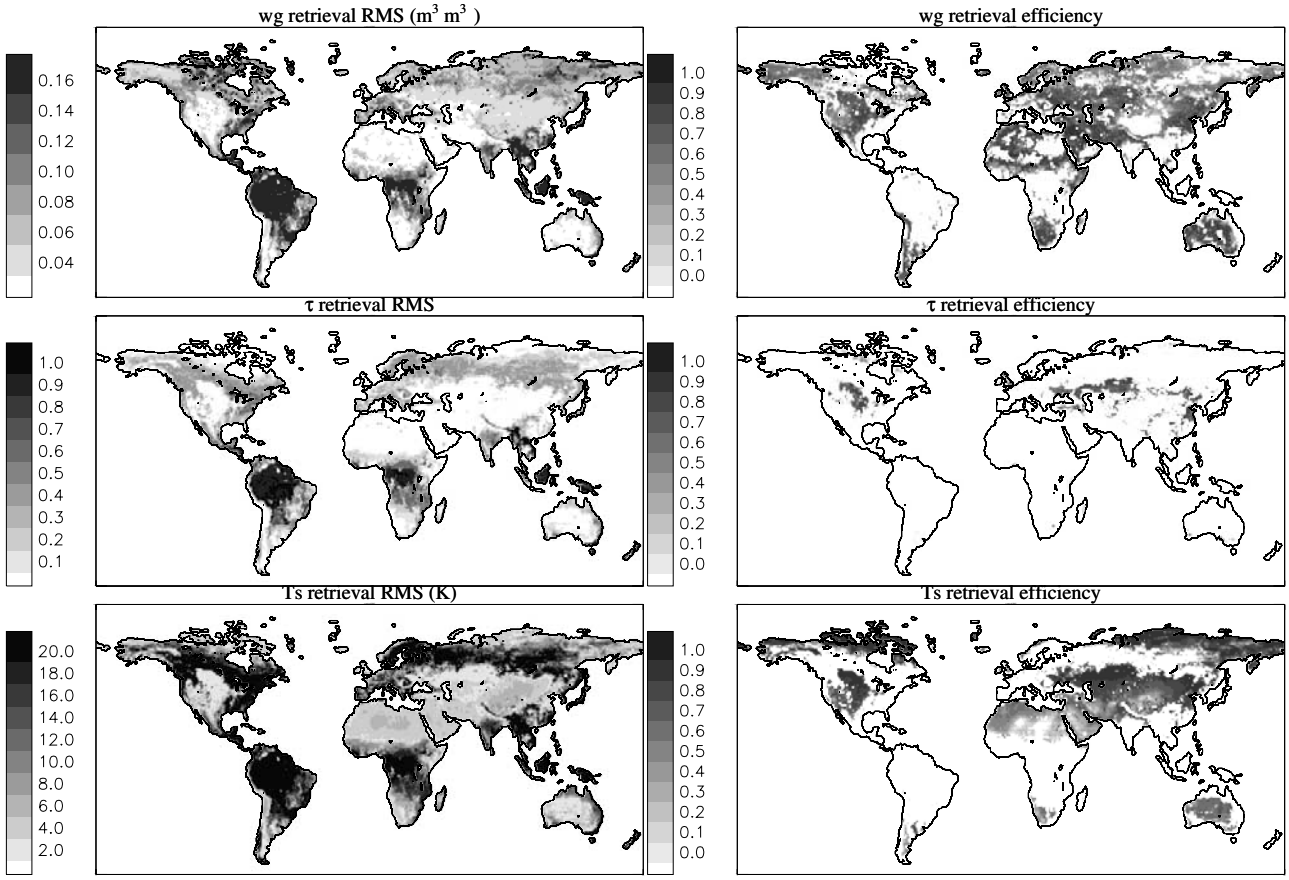

Figure 2. Spatial distribution of the 1988 retrieval (left) RMS error and (right) efficiency, of (from top to bottom) surface soil moisture, L-band optical thickness of the vegetation, surface temperature (wg, τ, T_S), using the IP1 algorithm with a 1 K noise on T_B. See color version of this figure at back of this issue.

the optimal observation time to minimize the Faraday effect [*Le Vine and Abraham*, 2002; *Yueh*, 2000].

[36] The scores employed to compare the reference and the retrieved temporal series are the RMS error and the efficiency (or skill score). The efficiency (E) of a method used to estimate a given variable v (in this study, $v = wg$, τ or T_S) is defined as:

$$E = 1 - \left[\frac{\sum_i (v_i - v_i^*)^2}{\sum_i (v_i - \mu)^2}\right] \text{ with } \mu = \frac{1}{N}\sum_{i=1}^{N} v_i \qquad (6)$$

where v_i and v_i^* are, the reference (i.e., the direct simulation) and the retrieved values of v, respectively. Positive values of E indicate that the employed method is more informative than prescribing a constant value of v equal to μ.

3. Results of the Three-Parameter Inversion

[37] The three-parameter retrievals were derived from either the IP1 or IP2 inversion processes. A significant advantage of retrieving 3 parameters (both τ and T_S, in addition to wg) is that a priori estimates of both τ and T_S, obtained from ancillary information, are not required in the retrieval process of wg. Therefore analyzing the obtained information about the time variations of land surface temperature or about the vegetation dynamics from the retrievals of T_S and τ, respectively, was not the central objective of this study. However, valuable information on these two variables were also obtained, and the most significant results are presented in this section.

3.1. Results of IP1

[38] For each continental pixel, a comparison between time series of reference (wg, τ and T_S) and retrieved (wg^*, τ^* and T_S^*) surface parameters was carried out for the IP1 inversion process. The spatial distribution of the values of the RMS error and efficiency that were computed for the three retrieved parameters are presented in Figure 2. The performance of the wg retrieval is presented in the two upper plots of Figure 2.

[39] Relatively good results were obtained over a large part of the globe. The wg^* accuracy appeared to be low in forested areas, especially in tropical regions (Amazonia, central Africa and Indonesia). In these regions, the RMS error was always higher than 0.16 m^3 m^{-3} (it was generally close to 0.25 m^3 m^{-3}) and the efficiency was negative. The low sensitivity of T_B to soil moisture was due to the high attenuation of the soil emission by the dense forest cover. This result could also be observed, to a lesser extent (the RMS error ranges between 0.08 and 0.12 m^3 m^{-3}), for boreal coniferous forests where the

forest biomass is significantly lower than in tropical regions. A low *wg** accuracy was also obtained over pixels where the cover fraction of water was significant, in particular in northern Canada, Scandinavia and eastern Russia (the RMS errors generally exceeded 0.16 $m^3\ m^{-3}$ for these pixels). The global yearly score ($\overline{RMS}$) computed as the average value of the RMS error obtained for all the pixels during a 1-year period was equal to 0.088 $m^3\ m^{-3}$. This score was significantly larger than the 0.04 $m^3\ m^{-3}$ accuracy threshold. However, if we consider only the pixels including less than 20 and 5% of forests and open water, respectively (which represents 45% of the pixels), the $\overline{RMS}$ value is brought down to 0.044 $m^3\ m^{-3}$. Therefore a 0.04 $m^3\ m^{-3}$ accuracy is reached over almost one half of the continental areas. Negative values of E (Figure 2, top right plot) were obtained over 40.0% of the continental area (white pixels). As expected, these regions corresponded to forested areas (tropical zones, boreal forests, eastern coast of the United States and Australia, western Europe), or regions including open water surfaces. Negative values of E were also obtained locally in desert areas (Sahara, Arabia) and on the Tibet plateau. These pixels corresponded to areas where the time variations in *wg* were weak. The RMS error of the *wg** associated to these pixels was rather low and the negative E was caused by a small bias.

[40] As far as retrievals of the optical depth (τ*) are concerned, a rather low accuracy was obtained in general: the global $\overline{RMS}$ error on τ* (Figure 2, middle left plot) was 0.264. If we consider that $b \approx 0.15$ and using equation (2), this value corresponds to an error of 1.8 kg m^{-2} in terms of vegetation water content, which is very high. A positive efficiency was obtained over only 10% of continental pixels (Figure 2, middle right plot). It can be also noted that the accuracy decreased as the pixel-averaged vegetation optical depth increased. The worst results were obtained over tropical forests (the RMS error was generally larger than 0.7). Poor results were obtained over broadleaf and coniferous forests (with RMS values ranging between 0.1 and 0.7) and relatively good results elsewhere. Over forested areas, the dependence of microwave emissivity on optical depth τ tends to saturate at levels of τ higher than about 1. Another explanation of the difficulty in retrieving τ over forested areas is the fact that the single scattering albedo ω was set to 0.05 in the inversion process (typical of grassland and agricultural areas) while this parameter was set at 0.15 for the reference simulations over forests. Analytically, almost the same values of T_B are obtained using ($\tau = 1.2$ and $\omega = 0.05$) or ($\tau = 1.5$ and $\omega = 0.15$). It follows that values of τ are always underestimated over forested areas. Results on T_S* suggest similar comments. The T_S * accuracy was low over forested areas (T_S was generally underestimated by about 20 K). RMS errors lower than 5 K were obtained over about 26% of the continental pixels.

[41] To illustrate the performance of IP1, a comparison between the time variations in reference and retrieved *wg*, τ and T_S is given for two pixels (Figures 3 and 4). The first one is almost exclusively composed of crops (95%, with a coniferous forest fraction of 5%) and located in central Europe close to the Black Sea (47.75°N, 38.25°E). The second one (referred to as Mississippi) is a mixed pixel located close to the Mississippi river (32.75°N; 92.75°W) including mostly coniferous forest (81%), crops (19%) and water (2%).

[42] A good agreement between reference and retrieved parameters was obtained for Black Sea pixel (Figure 3). The RMS error on *wg** during 1988 was 0.035 $m^3\ m^{-3}$. A peculiarity of this pixel is that during the three-month winter period (from December to February) the surface soil layer is totally frozen. During this period, the inversion process converged toward a minimum value of *wg** of about 0.07 $m^3\ m^{-3}$. This is due to the fact that the value of the permittivity of a frozen soil ($\varepsilon_{SF} = 5 - 0.5$ i) used in reference simulations corresponds to a low value of *wg* of 0.07 $m^3\ m^{-3}$ when using the routine computing the soil permittivity. It is thus difficult to distinguish a dry soil from a frozen soil in the soil moisture retrieval process. This specific point will be discussed in more detail in section 4. For the Black Sea pixel, the retrieval accuracy was satisfactory for both τ and T_S: the RMS error was 0.035 and 3.9 K, respectively, and E was larger than 0.7 in both cases.

[43] For the Mississippi pixel, the presence of forest led to a poor retrieval accuracy (Figure 4). All the variables (*wg*, τ and T_S) were underestimated. For example, the annual mean value of reference *wg* was 0.161 $m^3\ m^{-3}$ whereas the annual mean value of *wg** was 0.062 $m^3\ m^{-3}$, with a RMS error of 0.151 $m^3\ m^{-3}$. For τ and T_S, the mean bias was about 0.4 and 25 K, respectively. Note that this underestimation is a general result obtained for most of the pixels including a significant fraction of forests ($f_F > 10\%$). The E values were negative for all the parameters.

3.2. Results of IP2

[44] Using the IP2 process was a way to assess the impact of external information related to surface temperature. In IP2, the assumed accuracy on the T_S estimate was 2 K (σ_{Ts} was fixed to 2 K in the cost function C_F, instead of 15 K for IP1). This additional constraint in the retrieval process tended to force the retrieved T_S^* to be closer to the reference T_S.

[45] The spatial distribution of the RMS errors and efficiencies obtained using IP2 are given in Figure 5. It can be seen that low-accuracy areas remain (i.e., pixels including forests and open water areas). However, significantly better results than IP1 were obtained, mainly for *wg* and T_S. The global *wg** $\overline{RMS}$ error decreased significantly from 0.088 $m^3\ m^{-3}$ to 0.064 $m^3\ m^{-3}$. If pixels composed of less than 20% of forest and less than 5% of water are considered (i.e., 45% of the continental pixels), the global $\overline{RMS}$ value is 0.034 $m^3\ m^{-3}$ (0.044 $m^3\ m^{-3}$ for IP1). No major improvement was obtained for τ*. The $\overline{RMS}$ error on τ* decreased from 0.26 to 0.24. On the other hand, for the boreal coniferous forests, the RMS error decreased from 0.4–0.5 for IP1 down to 0.3–0.4 for IP2. Since T_S was constrained in IP2, improved values of T_S^* could be obtained but the $\overline{RMS}$ error was still high (6.9 K).

3.3. Comparing Different Retrieval Approaches

[46] To illustrate the improvement obtained by using IP2 instead of IP1, the time variations of reference and retrieved parameters are presented over the Mississippi pixel in Figure 6 (the corresponding results for IP1 are given in Figure 4). It can be seen that even though there is a rather

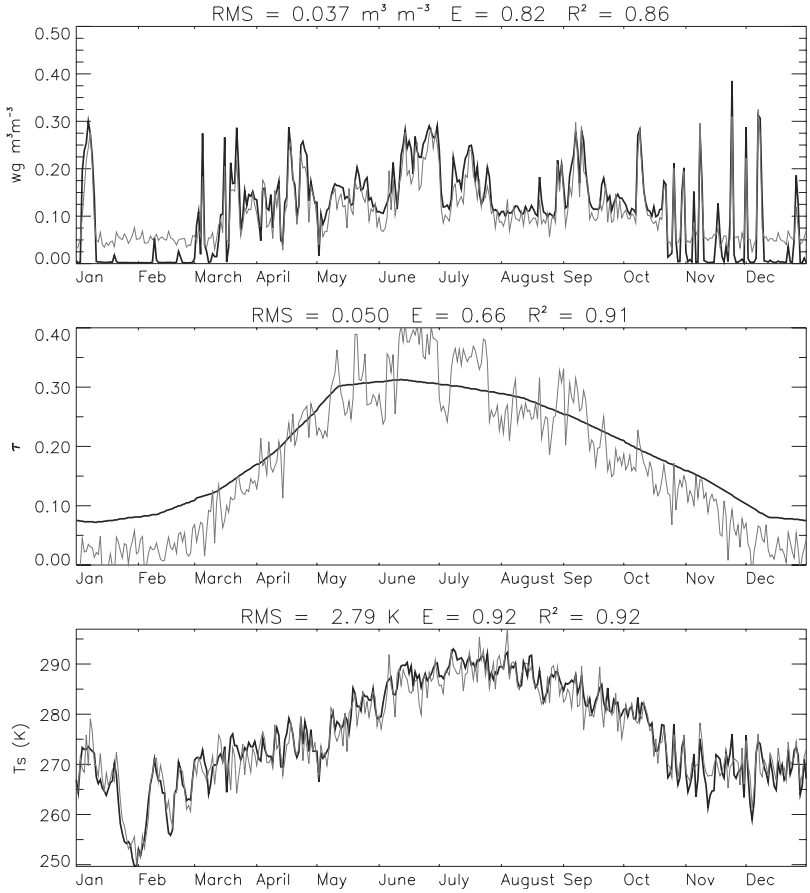

Figure 3. Time variation of reference and retrieved values (thick and fine lines, respectively) of surface soil moisture, L-band optical thickness of the vegetation, surface temperature (wg, τ, T_S) during 1988, over a crop pixel in central Europe (Black Sea), using the IP1 algorithm with a 1 K noise on T_B.

large underestimation of τ and T_S (RMS error of 0.37 and 16.3 K, respectively), wg* values are improved over forested areas using IP2, in contrast to IP1. The IP2 RMS error and E values were 0.058 m^3 m^{-3} and 0.34, respectively, and 0.15 m^3 m^{-3} and -3.6, respectively, for IP1.

[47] A global comparison of IP1 and IP2 is given in Figure 7. The probability density function of the different RMS errors is presented for both IP1 and IP2. These histograms synthesize the information on the RMS error as displayed in Figures 2 (for IP1) and 5 (for IP2). The vertical dash-dotted line in Figure 7a represents the 0.04 m^3 m^{-3} threshold on wg. It can be observed that IP2 provided a clear improvement of wg*. The 0.04 m^3 m^{-3} accuracy was reached for 39.3% of the continental pixels using IP2, and 21.5% using IP1. Note that for IP2, a large number of pixels still presented RMS error in the range 0.04–0.08 m^3 m^{-3}. In Figure 7b, it is difficult to assess whether IP2 provided any improvement in τ*. It can be noted that to the two peaks of the probability density of the RMS error, close to 0.4, correspond to coniferous forest areas. Slightly better retrievals could be obtained using IP2 over these pixels. Finally, a clear improvement on T_S^* was obtained (Figure 7c): RMS errors lower than 2 K on T_S retrievals do not occur using IP1 whereas they represent about 21% of the continental pixels using IP2. The $\overline{\text{RMS}}$ error on T_S decreased significantly, from 12.3 K to 6.9 K. Over forested areas, an underestimation of T_S exceeding 5 K was obtained (20 K for IP1).

[48] An inter-comparison of the results obtained using IP2 and LRM [*Pellarin et al.*, 2003] is given by Figure 8, for a 1 K T_B noise: the probability density functions of the wg* RMS errors are compared. It can be seen that significantly better results were obtained using LRM: the 0.04 m^3 m^{-3} accuracy was reached over about 90 and 40% of the pixels using LRM and IP2, respectively. The global $\overline{\text{RMS}}$ on wg* was 0.029 m^3 m^{-3} for LRM, and 0.064 m^3 m^{-3} for IP2. It should be noted that a direct comparison of these two methods is somewhat biased, since different assumptions were used to develop the two retrieval approaches. As noted above, in IP2, the retrievals were made assuming that little a priori information was available on the pixel land cover (most unfavorable conditions). Conversely, LRM was first calibrated over each pixel using reference T_B data in 1987. Thus all the information on the cover type and the soil texture was implicitly integrated in the calibrated coefficients of the pixel-based LRM regression. However, the LRM approach developed by *Pellarin et al.* [2003] was found to be significantly more sensitive to the radiometric noise than IP2. For instance, for a T_B noise increasing from 1 K to 3 K, the proportion of continental pixels where the soil moisture retrieval accuracy was better than 0.04 m^3 m^{-3} decreased from 90 to 25.4% for LRM and from 40 to 19.8% for IP2).

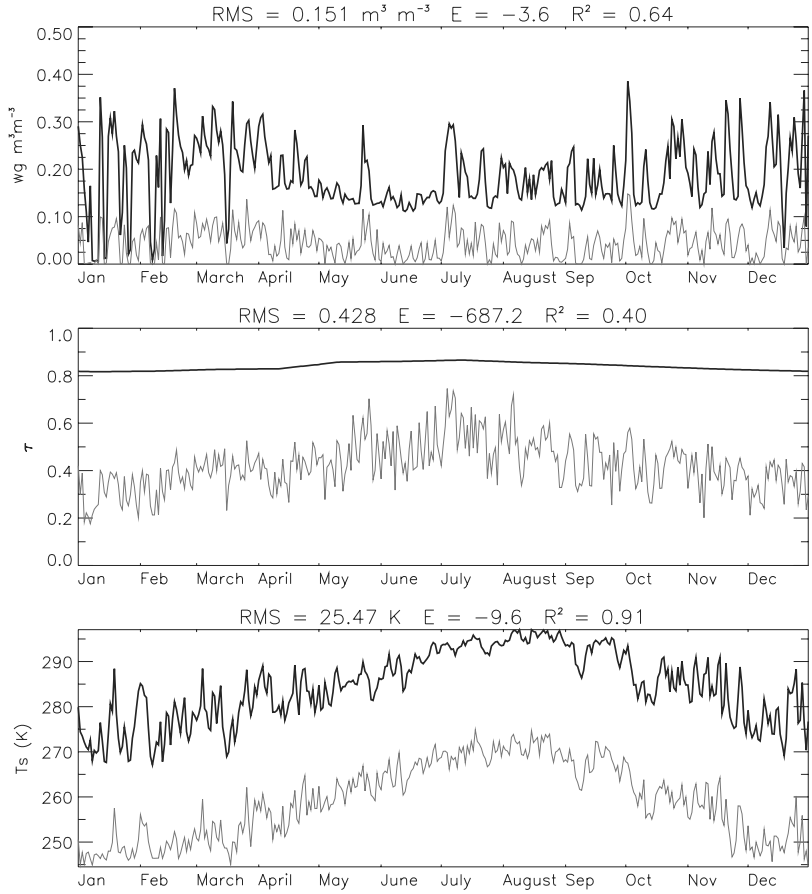

Figure 4. Time variation of reference and retrieved values (thick and fine lines, respectively) of surface soil moisture, L-band optical thickness of the vegetation, surface temperature (wg, τ, T_S) during 1988, over the Mississippi mixed pixel (coniferous forest 81%, crops 19% and water 2%),using the IP1 algorithm with a 1 K noise on T_B.

[49] The effect of various variables on the accuracy of forward model inversion is analyzed in more detail below.

3.4. Effect of State Variables

[50] The inversion's performance differed according to surface conditions (surface soil moisture and vegetation optical thickness). In particular, the frequency of wg* RMS error better than the 0.04 m^3 m^{-3} threshold (i.e., the success rate of the inversion) was not the same for different wg and τ values. Figure 9 shows the frequency distribution of wg and τ values, and the corresponding success rate, using IP2. It appears that (1) simultaneously large values of wg and τ, (2) very low values of wg, were associated with low success rates. In the first case, the weaker emission of a wet soil was more easily attenuated by the larger optical thickness of dense vegetation. In the second case, representative of soil freezing, the inversion produced biased wg*. For sparse vegetation (low τ), soil moisture had little effect on the success rate.

3.5. Effect of Soil Freezing and Snow

[51] As mentioned previously, the inversion process deteriorates in soil freezing conditions (Figure 3 and section 3.1). This is an important issue since in our simulations frozen soil surfaces can exceed 40% of the continental area at 0600 LST (e.g., in February). An attempt was made to detect soil freezing from the three-parameter retrievals. The simplest approach consisted in prescribing a T_S^* threshold below which the soil was considered as frozen. However, over forested areas, T_S was generally strongly underestimated (Figure 4) and soil freezing was erroneously diagnosed in many forested regions. Therefore it was attempted to detect soil freezing for pixels presenting low average values of τ*, only.

[52] Using IP1, it was found that, for τ* values lower than 0.2, the condition $T_S^* < 257$ K permitted to detect 56% of the soil freezing cases in 1988. In the same time, this method produced 4% of false detections. Using this crude indicator, and by setting $wg^* = 0$ m^3 m^{-3} when frozen soil conditions were detected, the global $\overline{\mathrm{RMS}}$ error decreased from 0.088 to 0.078 m^3 m^{-3}. The obtained improvement was particularly significant from November to April in the Northern Hemisphere.

[53] For IP2, for τ* values lower than 0.2, the condition was: $T_S^* < 266$ K. In this case, 73% of the soil freezing cases was detected, and the global $\overline{\mathrm{RMS}}$ error decreased from 0.064 to 0.049 m^3 m^{-3}. About 6% of false detections were obtained. These preliminary results show that a simple approach might be developed in the future to address the soil freezing issue, which is important to improve the wg retrieval.

[54] An attempt was made to detect snow by using a similar method. Using $T_S^* < 254$ K, $\tau^* < 0.4$, and $T_S^* < 260$ K,

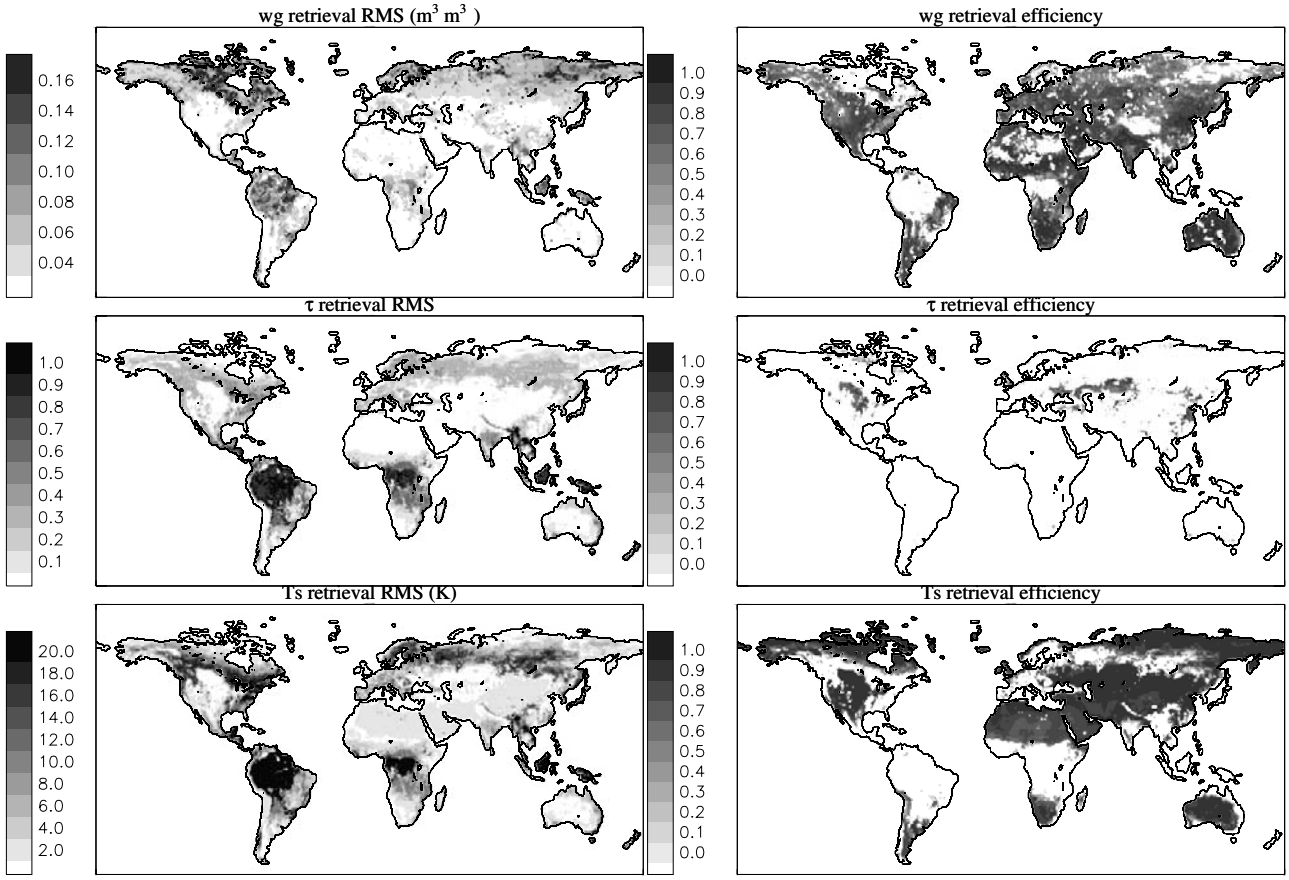

Figure 5. Spatial distribution of the 1988 retrieval (left) RMS error and (right) efficiency, of (from top to bottom) surface soil moisture, L-band optical thickness of the vegetation, surface temperature (wg, τ, T_S), using the IP2 algorithm with a 1 K noise on T_B. See color version of this figure at back of this issue.

$\tau^* < 0.6$ with IP1 and IP2, respectively, 45 and 49% of snow occurrence was detected, respectively. Although, in both configurations, less than 3% of false detections were made, it seems that detecting snow using this method is not accurate enough.

3.6. Effect of Open Water and Forest

[55] As shown in the previous section, the presence of forested and open water surfaces in the pixel is one of the key parameters affecting the wg^* accuracy. A quantitative assessment of this effect is given in Figure 10 for both IP1 and IP2. In Figure 10, the percentage of continental pixels for which the RMS error on wg^* is lower than a given RMS threshold (five thresholds were selected: 0.04, 0.06, 0.08, 0.12 and 0.16 $m^3\ m^{-3}$) is plotted as a function of the cover fraction of open water and forested surfaces. Note that the retrievals were not carried out for pixels presenting a water fraction exceeding 50%.

[56] A summary of the main features revealed in these four figures is given below:

[57] 1. For both IP1 and IP2, the presence of water surfaces within the pixel water cover constituted a significant limitation of the inversion process. For instance, when the water fraction exceeded 5% the percentage of pixels under the 0.04 $m^3\ m^{-3}$ error threshold was only 8 and 19% for IP1 and IP2, respectively. For water fraction values higher than 20%, the majority RMS errors were larger than 0.10 $m^3\ m^{-3}$.

[58] 2. IP2 was more efficient than IP1 for open-water free pixels. However, lower accuracies were obtained using IP2 for pixels including a significant proportion of water surfaces (more than 10%). The main explanation of this behavior is that the presence of water led to a significant decrease of T_B: this effect was interpreted by IP2 as resulting from the emission of very wet surfaces and leads to large overestimations of wg^*; conversely, in IP1, this was interpreted as resulting from the emission of cold areas and led to a large underestimation of T_S, with a limited effect on wg^*.

[59] 3. The presence of forested areas within the pixel was detrimental, to a lesser extent than for open water surfaces, to the quality of both IP1 and IP2 [see also *Van de Griend et al.*, 2003]. For instance, for a forest fraction of 0.2, the percentage of pixels under the 0.04 $m^3\ m^{-3}$ threshold was still about 10 and 50% for IP1 and IP2, respectively, whereas this percentage was almost zero for a fractional water cover of 0.2 (Figure 10).

[60] 4. Over forested areas, IP2 performed better than IP1. In IP1, the presence of forested areas within the pixel led to the underestimation of all 3 parameters (wg^*, τ^*, T_S^*) in the retrieval process (see Figure 4, for example). The T_S constraint of IP2, allowed to limit the drift of T_S^* toward

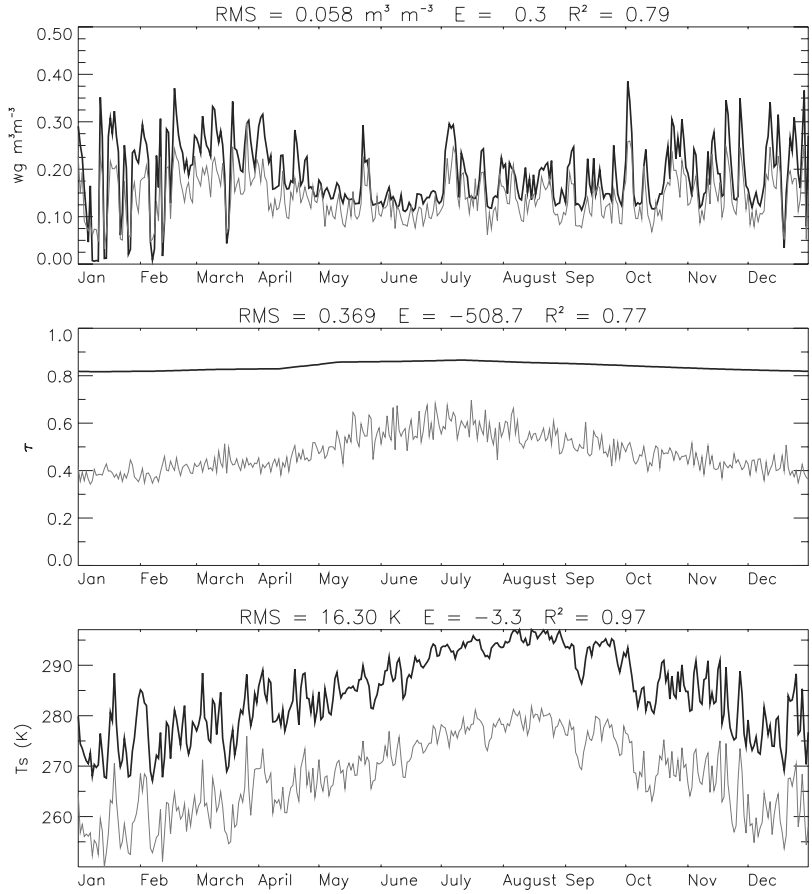

Figure 6. Time variation of reference and retrieved values (dark and grey lines, respectively) of surface soil moisture, L-band optical thickness of the vegetation, surface temperature (wg, τ, T_S) during 1988, over the Mississippi mixed pixel (coniferous forest 81%, crops 19% and water 2%),using the IP2 algorithm with a 1 K noise on T_B.

low values, and a better accuracy could be obtained on wg* (Figure 6).

3.7. Effect of Instrumental Noise

[61] In section 3, IP1 and IP2 retrievals were obtained for a 1 K noise, a value representative of the expected performance of SMOS. The effect of larger noise levels on T_B was investigated. Figure 11 presents histograms of the RMS error on wg*, τ* and T_S^* by using IP1 and IP2, for 3 noise levels: 1, 2 and 3 K. In Figure 11, it can be noted that noise induced a decrease in the wg* accuracy, and the impact of T_B noise was less pronounced for IP2 than for IP1.

[62] For IP2 and for the 3, 2, and 1 K noise levels, a RMS error on wg* lower than 0.04 m^3 m^{-3} was obtained for only 19.8, 35.2 and 39.3% of the pixels, respectively. The general shape of the 3 curves is rather constant, but the minimum error on wg* increased of about 0.01 m^3 m^{-3} for each 1 K increment in the T_B noise.

[63] The effect of the T_B noise on the τ retrievals was much lower, for both IP1 and IP2. The global $\overline{\text{RMS}}$ increased from 0.25 (for a 1 K noise level) to 0.28 and 0.29 (2 and 3 K, respectively).

[64] Conversely, increasing T_B noise levels produced a significant decrease of the T_S^* accuracy. However, IP1 and IP2 reacted differently to this effect. For IP1, the $\overline{\text{RMS}}$ increased from 8.6 K (for a 1 K noise level) to 9.5 and 10.32 K (2 and 3 K, respectively). For IP2, the $\overline{\text{RMS}}$ decreased, surprisingly, from 6.9 K (for a 1 K noise level) to 3.6 and 2.6 K (2 and 3 K, respectively). This behavior was due to the fact that as the T_B noise level increased, σ_{TB} increased in equation (5), and the weight of the last term in this equation became more important. In other words, as the T_B noise level increased, the constraint on T_S included in equation (5) became stronger, relative to the other terms. Therefore the RMS error on T_S^* tended toward 2 K, which corresponds to the uncertainty associated with the estimates of surface temperature (T_S^{ini}) which was introduced in IP2.

4. Discussion and Conclusion

[65] In this study, the performance of a three-parameter inversion process, using little ancillary information, was evaluated at the global scale, during one annual cycle. The obtained results contribute to better define the potential of future L-band spaceborne missions such as SMOS for monitoring soil moisture at the global scale, using a method which could pave the way for the development of an operational algorithm. This first-step approach may be improved in future studies by considering specific targets for which additional information is available.

[66] While the study of *Wigneron et al.* [2000] analyzed the retrievals over four types of homogeneous scenes, the

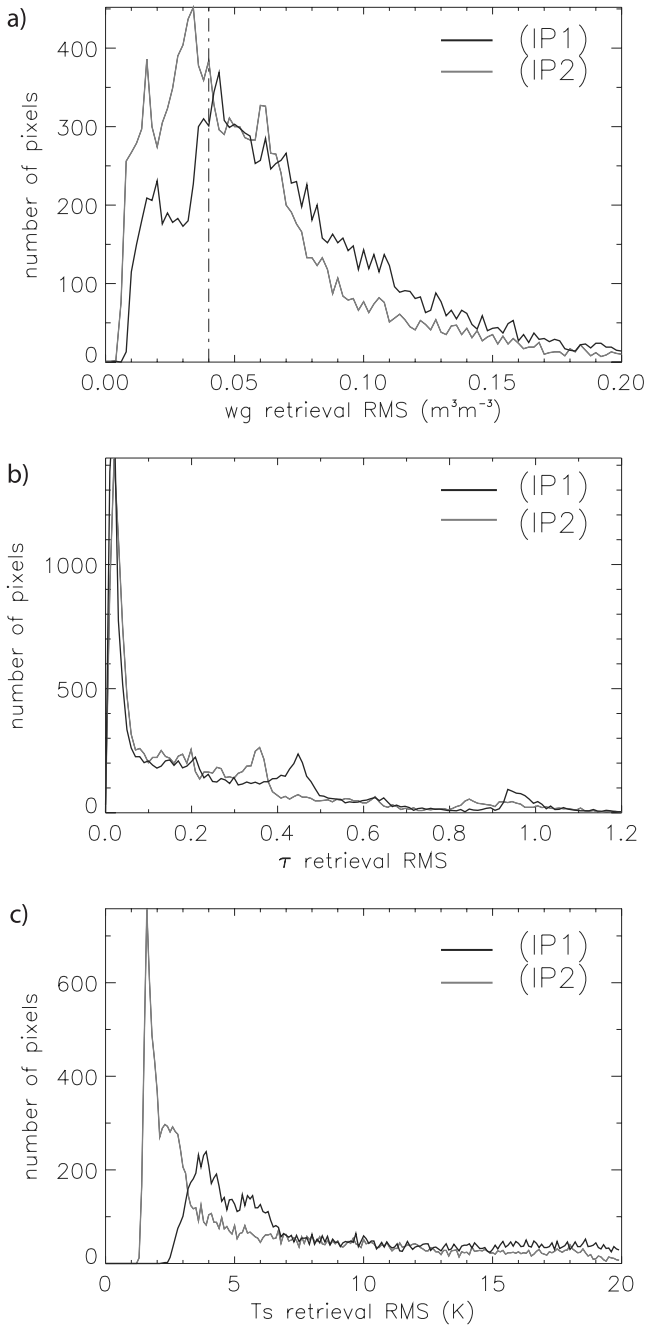

Figure 7. Probability density function of the 1988 retrieval RMS error of (a) surface soil moisture, (b) L-band optical thickness of the vegetation, and (c) surface temperature (wg, τ, T_S), using IP1 and IP2 algorithms (dark and grey lines, respectively) with a 1 K noise on T_B. The vertical dash-dotted line represents the 0.04 m^3 m^{-3} threshold on wg.

present paper was based on a global synthetic dual-polarized, multiangular L-band T_B data set (Pellarin et al., submitted manuscript, 2003) describing the continental pixels at a half-degree spatial resolution during 2 years and accounting for within-pixel heterogeneity, using 1 km resolution land cover maps. On the basis of this large data set, a detailed analysis of the capability of monitoring soil moisture from T_B could be performed. Global maps of the retrieval accuracy for 3 main variables, wg, τ and T_S were obtained. Two versions of the three-parameter retrieval approach were used: IP1, using no a priori information, and IP2, using surface temperature estimates. In both cases, it was assumed that no a priori information about the pixel land cover was available. This worst-case assumption was made in order to simulate uncontrolled operational conditions and limit the circularity problem of using the same model to produce the synthetic T_B and to perform the inversion. Also, events such as flooding or fire may lead to quick changes in the land cover, and an algorithm using a lot of a priori information would then have difficulties. In spite of using a synthetic data set, we are rather confident of our results because (i) the L-MEB model was validated as much as possible (see section 2.2), (ii) the validation of three-parameter retrievals over experimental data has been evaluated by *Wigneron et al.* [1995, 2002b] over soybean, wheat and corn canopies and in two ongoing studies (M. Pardé et al., Using passive multi-angular and bi-polarization microwave measurements to retrieve soil moisture over a wheat field, Comparison of different methods, submitted to *Remote Sensing of Environment*, 2003; M. Pardé et al., N-parameter retrievals from L-band microwave measurements over a variety of agricultural crops, manuscript in preparation, 2003) over a variety of vegetation canopies. The experimental data used in these studies were obtained during a complete vegetation cycle (from bare soil to harvest in some cases) over a large range of land surface conditions. The error of the retrieved wg ranged between 0.030 and 0.055 m^3 m^{-3}. These values are close to those obtained in the present study over pixels presenting a low forest cover fraction

[67] The most significant results of this study are given below:

[68] 1. The soil moisture retrieval accuracy was better than 0.04 m^3 m^{-3} (which is the optimal accuracy for potential applications) over about 20% and 40% of the continental areas for IP1 and IP2, respectively. The accuracy of τ retrievals was generally rather low for both IP1 and IP2.

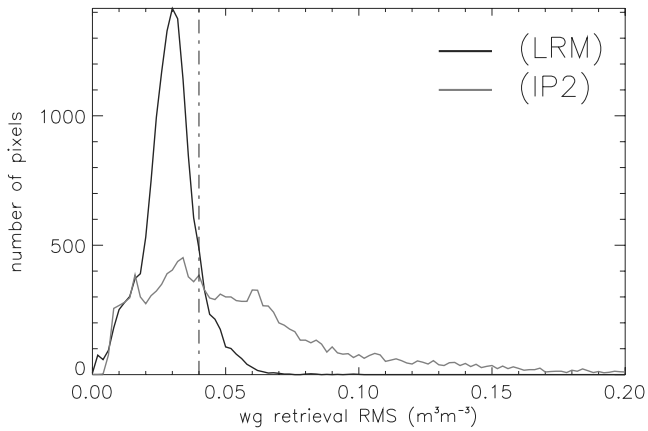

Figure 8. Probability density function of the 1988 retrieval RMS error of surface soil moisture (wg), using LRM [*Pellarin et al.*, 2003] and IP2 algorithms (dark and grey lines, respectively) with a 1 K noise on T_B. The vertical dash-dotted line represents the 0.04 m^3 m^{-3} threshold on wg.

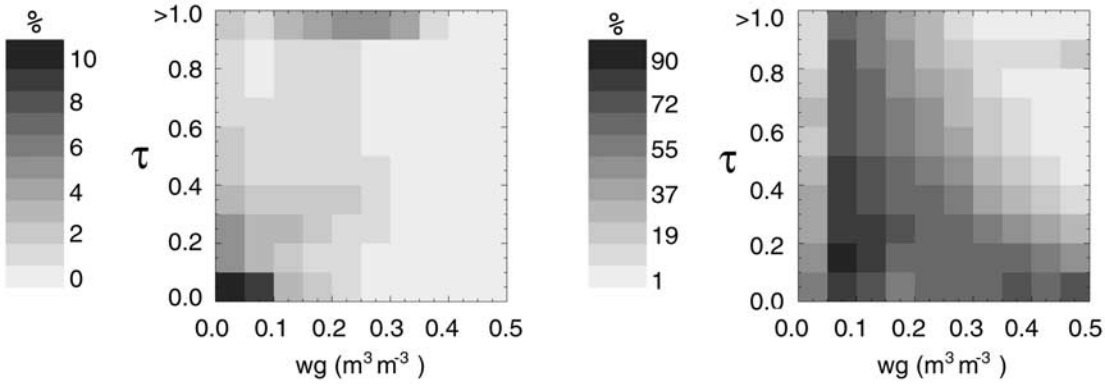

Figure 9. Effect of state variables on the IP2 inversion: (left) frequency distribution (%) of surface soil moisture and vegetation L-band optical thickness (*wg* and τ, respectively) and (right) the corresponding success rate (%), i.e., the frequency of *wg** RMS error better than the 0.04 m^3 m^{-3} threshold.

However, RMS errors on τ lower than 0.15 (corresponding to a value of vegetation water content of about 1 kg m^{-2}) were obtained over 49% of the continental areas. Most often than not, the three-parameter retrieval approach IP1 could not provide accurate estimates of surface temperature T_S. Results of IP2 were produced assuming that estimates of T_S with 2 K accuracy could be obtained at the global scale. Estimation of T_S with such an accuracy is feasible, from both satellite measurements and weather forecast analyses including a land surface scheme [*Jin and Dickinson*, 2002]. On the

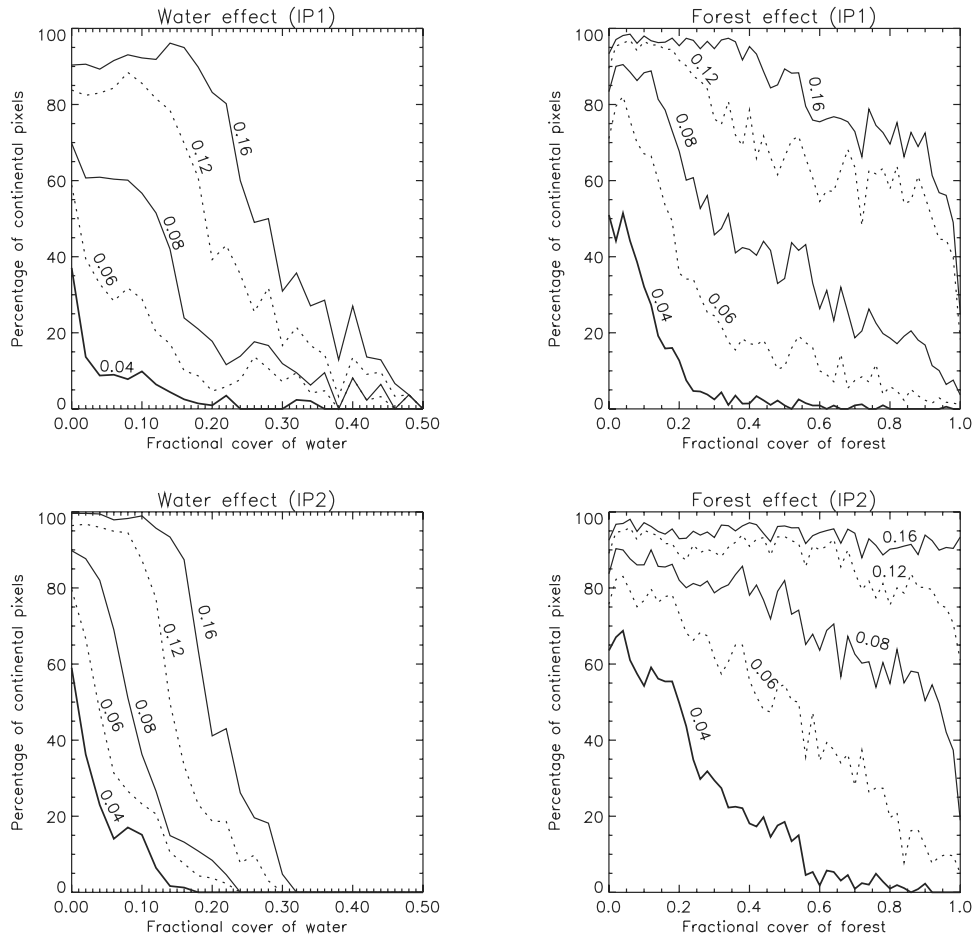

Figure 10. Percentage of continental pixels for which the 1988 retrieval RMS error of surface soil moisture is lower than a given RMS threshold (0.04, 0.06, 0.08, 0.12 or 0.16 m^3 m^{-3}) as a function of the cover fraction of (left) open water and (right) forested surfaces, for (top) IP1 and (bottom) IP2 algorithms, with a 1 K noise on T_B.

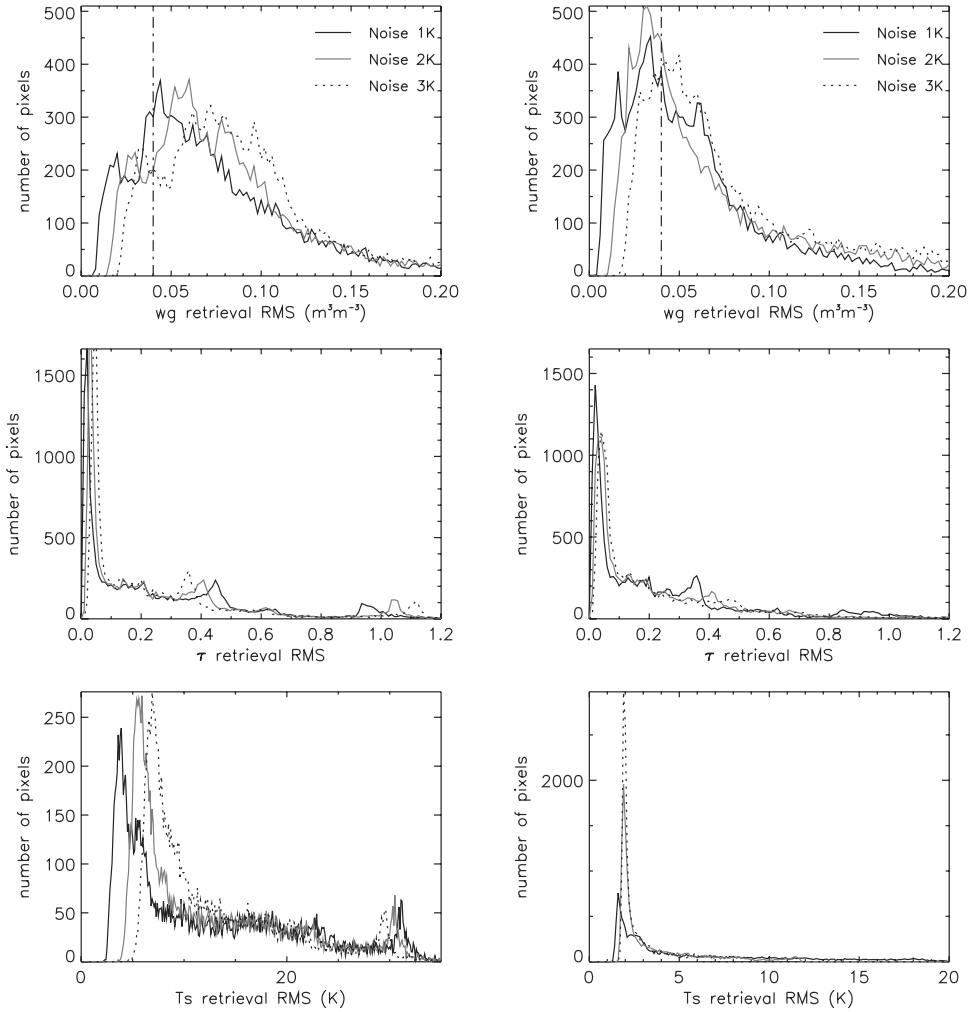

Figure 11. Probability density function of the 1988 retrieval RMS error of (from top to bottom) surface soil moisture, L-band optical thickness of the vegetation, surface temperature (wg, τ, T_S), using (left) IP1 and (right) IP2 algorithms for different noise levels on T_B: 1, 2 and 3 K (dark, grey and dotted lines, respectively). The vertical dash-dotted line represents the 0.04 m^3 m^{-3} threshold on wg.

basis of this result, and considering that, in the real world, vertical temperature gradients are likely to affect the soil-vegetation system, it can be concluded that trying to retrieve T_S from L-band emission observations is worthless. T_S should be fixed to its first guess value during the retrieval process.

[69] 2. IP2 was compared with the LRM approach, which is a simpler method estimating wg from a linear combination of microwave indices derived from the multiangular and dual-polarization T_B data [*Pellarin et al.*, 2003]. Significantly better results were obtained using LRM, since the 0.04 m^3 m^{-3} accuracy could be reached over about 90% of the pixels and the global $\overline{\text{RMS}}$ on wg was 0.029 m^3 m^{-3} compared with 40% and 0.064 m^3 m^{-3} for IP2, respectively. However, LRM was calibrated using reference T_B data in 1987 and all the pixel land cover, soil texture, and climate characteristics were implicitly integrated in LRM. In other words, a lot of a priori information was included in LRM, while IP2 used only T_S estimates.

[70] 3. At the global scale, the retrieval accuracy was found to be related to the land surface characteristics. In particular, neglecting to explicitly account for the fractional cover of open water, forests, and soil freezing, was detrimental to the soil moisture retrieval accuracy. It was found that the least constrained method (IP1) was less sensitive to this effect. The reason is that the use of a priori information is delicate: a constrained inversion algorithm is likely to produce erroneous results if the used a priori information is not correct. However, an operational inversion algorithm should account for the available information, especially about the extent of open water surfaces included into the pixel. Studies are ongoing to evaluate to which accuracy level this effect should be quantified, by accounting for the SMOS characteristics: the changing footprint size as a function of the view angle, the complex multiangular configuration [*Waldteufel et al.*, 2000].

[71] **Acknowledgments.** The authors wish to thank ESA and CNES for supporting this work, V. Masson for providing the ECOCLIMAP database, and M. Berger (ESA/ESTEC) for his helpful comments concerning the manuscript, as well as the anonymous reviewers. This work was supported by a grant from the European Space Agency (ESA).

References

Brunfeldt, D. R., and F. T. Ulaby, Measured microwave emission and scattering in vegetation canopies, *IEEE Trans. Geosci. Remote Sens.*, *22*, 520–524, 1984.

Brunfeldt, D. R., and F. T. Ulaby, Microwave emission from row crops, *IEEE Trans. Geosci. Remote Sens.*, *24*, 353–359, 1986.

Calvet, J.-C., and J. Noilhan, From near-surface to root-zone soil moisture using year-round data, *J. Hydrometeorol.*, *1*(5), 393–411, 2000.

Cognard, A.-L., C. Loumagne, M. Normand, P. Olivier, C. Ottlé, D. Vidal-Madjar, S. Louahala, and A. Vidal, Evaluation of the ERS 1/synthetic aperture radar capacity to estimate surface soil moisture: Two-year results over the Naizin watershed, *Water Resour. Res.*, *31*(4), 975–982, 1995.

Dirmeyer, P. A., Using a global soil wetness dataset to improve seasonal climate simulation, *J. Clim.*, *13*, 2900–2922, 2000.

Entekhabi, D., H. Nakamura, and E. G. Njoku, Solving the inverse problem for soil moisture and temperature profiles by sequential assimilation of multifrequency remotely sensed observations, *IEEE Trans. Geosc. Remote Sens.*, *32*, 438–447, 1994.

Fennessy, M. J., and J. Shukla, Impact of initial soil wetness on seasonal atmospheric prediction, *J. Clim.*, *12*, 3167–3180, 1999.

Ferrazzoli, P., L. Guerriero, and J.-P. Wigneron, Simulating L-band emission of forests in view of future satellite applications, *IEEE Trans. Geosci. Remote Sens.*, *40*, 2700–2708, 2002.

Jackson, T. J., and T. J. Schmugge, Vegetation effects on the microwave emission of soils, *Remote Sens. Environ.*, *36*, 203–212, 1991.

Jackson, T. J., D. M. Le Vine, C. T. Swift, T. J. Schmugge, and F. R. Schiebe, Large area mapping of soil moisture using the ESTAR passive microwave radiometer in Washita'92, *Remote Sens. Environ.*, *53*, 27–37, 1995.

Jackson, T. J., D. M. Le Vine, A. Y. Hsu, A. Oldak, P. J. Starks, C. T. Swift, J. D. Isham, and M. Haken, Soil moisture mapping at regional scales using microwave radiometry: The Southern Great Plains Hydrology Experiment, *IEEE Trans. Geosci. Remote Sens.*, *37*, 2136–2150, 1999.

Jin, M., and R. E. Dickinson, New observational evidence for global warming from satellite, *Geophys. Res. Lett.*, *29*(10), 1400, doi:10.1029/2001GL013833, 2002.

Kerr, Y. H., P. Waldteufel, J.-P. Wigneron, J. Font, and M. Berger, Soil moisture retrieval from space: The Soil Moisture and Ocean Salinity (SMOS) mission, *IEEE Trans. Geosci. Remote Sens.*, *39*, 1729–1735, 2001.

Leese, J., T. Jackson, A. Pitman, and P. Dirmeyer, GEWEC/BAHC International Workshop on soil moisture monitoring, analysis, and prediction for hydrometeorological and hydroclimatological applications, *Bull. Am. Meteorol. Soc.*, *82*, 1423–1430, 2001.

Le Vine, D. M., and S. Abraham, The effect on remote sensing of the sea surface salinity from space: Absorption and emission at L-band, *IEEE Trans. Geosci. Remote Sens.*, *40*, 771–782, 2002.

Marquardt, D. W., An algorithm for least-squares estimation of nonlinear parameters, *J. Soc. Ind. Appl. Math.*, *11*, 431–444, 1963.

Masson, V., J. L. Champeaux, F. Chauvin, C. Meriguet, and R. Lacaze, A global database of land surface parameters at 1 km resolution in meteorological and climate models, *J. Clim.*, *16*, 1261–1282, 2003.

Meeson, B. W., F. E. Corprew, J. M. P. McManus, D. M. Myers, J. W. Closs, K.-J. Sun, D. J. Sunday, and P. J. Sellers, ISLSCP Initiative I: Global data sets for land-atmosphere models, 1987–1988 [CD-ROM], vols. 1–5, NASA Goddard Space Flight Cent. Distrib. Active Arch. Cent., Greenbelt, Md., 1995.

Mo, T., B. J. Choudhury, T. J. Schmugge, J. R. Wang, and T. J. Jackson, A model for microwave emission from vegetation-covered fields, *J. Geophys. Res.*, *87*, 11,229–11,237, 1982.

Njoku, E. G., and L. Li, Retrieval of land surface parameters using passive microwave measurements at 6–18 GHz, *IEEE Trans. Geosci. Remote Sens.*, *37*, 79–93, 1999.

Noilhan, J., and J.-C. Calvet, Mesoscale land-atmosphere models and data needs, in *Passive Microwave Remote Sensing of Land-Atmosphere Interactions, ESA/NASA International Workshop, St. Lary, 1993*, pp. 17–54, edited by B. J. Choudhury et al., VSP, Utrecht, 1995.

Noilhan, J., and S. Planton, A simple parameterization of land surface processes for meteorological models, *Mon. Weather Rev.*, *117*, 536–549, 1989.

Owe, M., R. de Jeu, and J. Walker, A methodology for surface soil moisture and vegetation optical depth retrieval using the microwave polarization difference index, *IEEE Trans. Geosci. Remote Sens.*, *39*, 1643–1654, 2001.

Pampaloni, P., and S. Paloscia, Microwave emission and plant water content: A comparison between field measurements and theory, *IEEE Trans. Geosci. Remote Sens.*, *24*, 900–905, 1986.

Pellarin, T., J.-C. Calvet, and J.-P. Wigneron, Surface soil moisture retrieval from L-band radiometry: A global regression study, *IEEE Trans. Geosci. Remote Sens.*, in press, 2003.

Pulliainen, J., and M. Hallikainen, Retrieval of regional snow water equivalent from space-borne passive microwave observations, *Remote Sens. Environ.*, *75*, 76–85, 2001.

Pulliainen, J., J.-P. Kärnä, and M. Hallikainen, Development of geophysical retrieval algorithms for the MIMR, *IEEE Trans. Geosci. Remote Sens.*, *31*, 268–277, 1993.

Pulliainen, J., J. Grandell, and M. Hallikainen, HUT snow emission model and its applicability to snow water equivalent retrieval, *IEEE Trans. Geosci. Remote Sens.*, *37*, 1378–1390, 1999.

Schmugge, T. J., and T. J. Jackson, Mapping soil moisture with microwave radiometers, *Meteorol. Atmos. Phys.*, *54*, 213–223, 1994.

Van de Griend, A. A., and M. Owe, Determination of microwave vegetation optical depth and single scattering albedo from large scale soil moisture and Nimbus/SMMR satellite observations, *Int. J. Remote Sens.*, *14*(10), 1875–1886, 1993.

Van de Griend, A. A., and M. Owe, The influence of polarization on canopy transmission properties at 6. 6 GHz and implications for large scale soil moisture monitoring in semi-arid environments, *IEEE Trans. Geosci. Remote Sens.*, *32*, 409–415, 1994.

Van de Griend, A. A., J.-P. Wigneron, and P. Waldteufel, Consequences of surface heterogeneity for parameter retrieval from 1.4 GHz multi-angle SMOS observations, *IEEE Trans. Geosci. Remote Sens.*, in press, 2003.

Waldteufel, P., E. Anterrieu, J. M. Goutoule, and Y. Kerr, Field of view characteristics of a microwave 2-D interferometric antenna, as illustrated by the MIRAS concept, in *Microwave Radiometry and Remote Sensing of the Earth's Surface and Atmosphere*, edited by P. Pampaloni and S. Paloscia, pp. 477–483, VSP, Utrecht, 2000.

Wang, J. R., and B. J. Choudhury, Remote sensing of soil moisture content over bare field at 1.4GHz frequency, *J. Geophys. Res.*, *86*, 5277–5282, 1981.

Wang, J. R., J. C. Shiue, T. J. Schmugge, and E. T. Engman, The L-band PBMR measurements of surface soil moisture in FIFE, *IEEE Trans. Geosci. Remote Sens.*, *28*, 906–913, 1990.

Wigneron, J.-P., A. Chanzy, J.-C. Calvet, and N. Bruguier, A simple algorithm to retrieve soil moisture and vegetation biomass using passive microwave measurements over crop fields, *Remote Sens. Environ.*, *51*, 331–341, 1995.

Wigneron, J.-P., P. Waldteufel, A. Chanzy, J.-C. Calvet, and Y. Kerr, Two-D microwave interferometer retrieval capabilities of over land surfaces (SMOS Mission), *Remote Sens. Environ.*, *73*, 270–282, 2000.

Wigneron, J.-P., L. Laguerre, and Y. Kerr, Simple modeling of the L-band microwave emission from rough agricultural soils, *IEEE Trans. Geosci. Remote Sens.*, *39*, 1697–1707, 2001.

Wigneron, J.-P., A. Chanzy, J.-C. Calvet, A. Olioso, and Y. Kerr, Modeling approaches to assimilating *L* band passive microwave observations over land surfaces, *J. Geophys. Res.*, *107*(D14), 4219, doi:10.1029/2001JD000958, 2002a.

Wigneron, J.-P., Y. Kerr, J.-C. Calvet, T. Pellarin, and S. Schmidl Sobjaerg, Monitoring land surface soil moisture from L-band microwave radiometry: Retrievals from multi-angular observations, paper presented at First International Symposium on Recent Advances in Quantitative Remote Sensing, Univ. de Valencia, Torrent, Spain, 16–20 Sept. 2002b.

Wood, E. F., D.-S. Lin, P. A. Troch, M. Mancini, and T. J. Jackson, Soil moisture estimation: Comparisons between hydrologic model estimates and remotely sensed estimates, in *Passive Microwave Remote Sensing of Land-Atmosphere Interactions, ESA/NASA International Workshop, St. Lary, 1993*, edited by B. J. Choudhury et al., pp. 17–54, VSP, Utrecht, 1995.

Yueh, S. H., Estimates of Faraday rotation with passive microwave polarimetry for microwave remote sensing of earth surfaces, *IEEE Trans. Geosci. Remote Sens.*, *38*, 2434–2438, 2000.

J.-C. Calvet and T. Pellarin, CNRM-GAME, Météo-France, URA CNRS 1357, 31057 Toulouse Cedex 1, France. (calvet@meteo.fr)

P. Waldteufel, Service d'Aéronomie, IPSL, 91371 Verrières le Buisson, France.

J.-P. Wigneron, Unité de Bioclimatologie, INRA, BP81, 33883, Villenave d'Ornon, France.

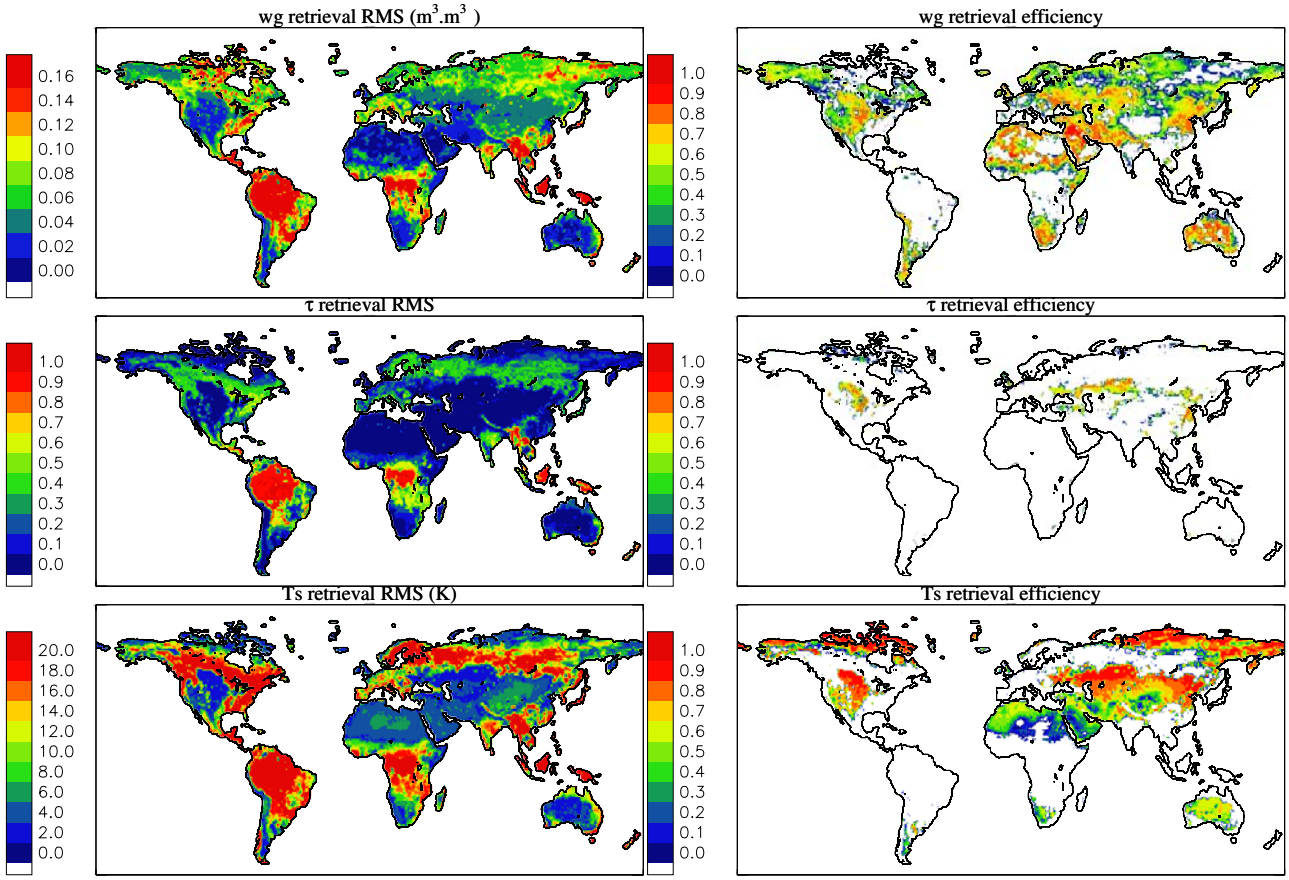

Figure 2. Spatial distribution of the 1988 retrieval (left) RMS error and (right) efficiency, of (from top to bottom) surface soil moisture, L-band optical thickness of the vegetation, surface temperature (wg, τ, T_S), using the IP1 algorithm with a 1 K noise on T_B.

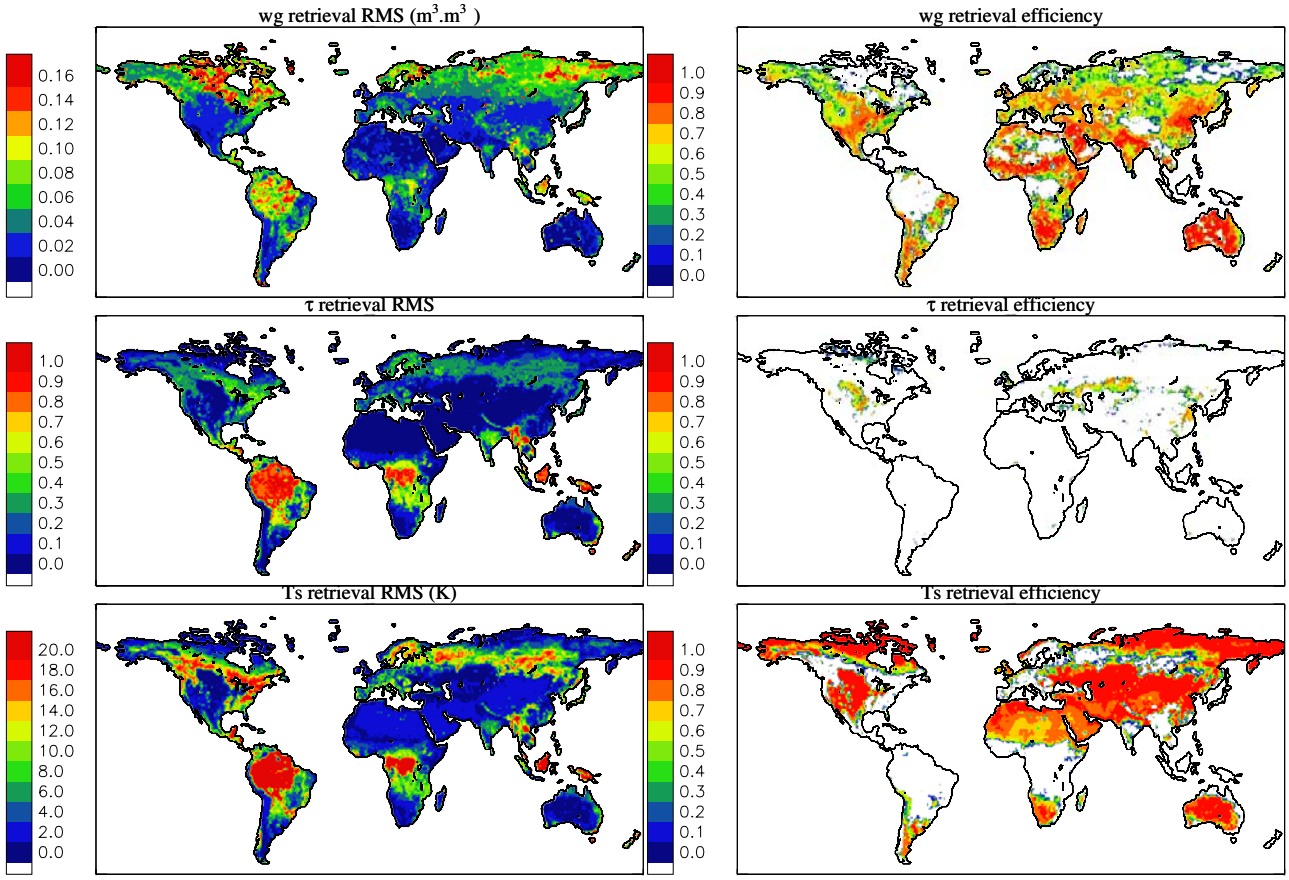

Figure 5. Spatial distribution of the 1988 retrieval (left) RMS error and (right) efficiency, of (from top to bottom) surface soil moisture, L-band optical thickness of the vegetation, surface temperature (wg, τ, T_S), using the IP2 algorithm with a 1 K noise on T_B.